PROCEEDINGS OF SPIE

SPIEDigitalLibrary.org/conference-proceedings-of-spie

Hyperspectral detection of methane stressed vegetation

Margot Accettura, Tim Bauch, Nina Raqueño, Joe Mallia, Carl Salvaggio

Margot Accettura, Tim Bauch, Nina Raqueño, Joe Mallia, Carl Salvaggio, "Hyperspectral detection of methane stressed vegetation," Proc. SPIE 10664, Autonomous Air and Ground Sensing Systems for Agricultural Optimization and Phenotyping III, 106640I (21 May 2018); doi: 10.1117/12.2304045

SPIE.

Event: SPIE Commercial + Scientific Sensing and Imaging, 2018, Orlando, Florida, United States

Hyperspectral detection of methane stressed vegetation

Margot Accettura[a], Timothy Bauch[a], Nina Raqueño[a], Joseph Mallia[b], and Carl Salvaggio[a]

[a]Rochester Institute of Technology, 54 Lomb Memorial Drive, Rochester, NY, 14623, USA
[b]NYSEARCH, 20 Waterview Blvd., Parsippany, NJ, 07054, USA

ABSTRACT

This study examines the hyperspectral reflectance characteristics of vegetation stressed by the influence of low-level sub-terrainean methane leakage from buried pipelines. The purpose is to ascertain whether high-spatial resolution spectral imagery can be used to geolocate small methane leaks in imagery collected from small unmanned aerial systems (sUAS). This could lead to rapid detection of methane leaks by finding spectrally unique regions of stressed vegetation which might benefit a variety of industries including utility inspectors, grounds maintenance crews, and construction personnel. This document describes an experiment to manually stress vegetation by introducing methane at a low flow rate beneath a layer of turf, allowing it to percolate to the surface and affect the vitality of the overlying turf. For comparison, a turf plot was stressed by root rot caused by over-watering, as well as a sample of turf used as a control area (healthy grass). The three areas of vegetation were observed daily over the course of a one-month period with a ground spectrometer to determine the onset and time line of damage to the vegetation. High-spatial resolution spectral imagery was also collected each day to observe wavelength characteristics of the damage. First derivative analysis was used alongside physiology-based indices and logistic regression to detect differences between healthy and stressed vegetation. The hyperspectral data showed that as vegetation is stressed the red-edge slope decreases along with values through the near infrared (NIR) while the short wave infrared (SWIR) region increases. The normalized difference index (NDI) calculation of stressed vegetation in relation to healthy vegetation is maximum using a ratio of reflectance values at 750 and 1910 nm. Conclusions will be presented as to whether sUAS may be used to determine if vegetation stressed by methane can be easily detected and which spectral bands are most effective for spotting this particular stressor.

Keywords: hyperspectral, remote sensing, sUAS, methane, vegetation stress

1. INTRODUCTION

The hyperspectral signature of the reaction between methane and vegetation is an important measure for various industries. The reason for vegetation health deterioration from methane is because methane interacts with and stresses the roots of the vegetation. This stress is believed to be caused by a few indirect reactions with the soil. The most accepted reasoning is the amount of methane in the soil displaces soil-oxygen and deprives the roots of necessary oxygen. Another potential cause of stress is the methane interacting with bacteria and other natural processes in the soil thus leading to stress from variations in the natural soil environment. A final explanation is that the dryness of the methane leads to less moisture content in the soil.[1,2] A lack of oxygen, being the probable primary cause of methane stress, leads to less energy for root growth, making it harder for roots to get necessary water and nutrients from the soil.

The presence of methane is an external stressor on the overlaying turf. In order to differentiate between unnatural stress and stress caused by natural effects, one of the study areas of turf was subjected to root rot. There are two potential sources for root rot. The first, carried out during this experiment, is severe over-watering and insufficient drainage that leaves the root system drowned and lacking oxygen. The second cause of root rot is wet conditions in the vegetation that cause different forms of fungus to flourish and rot the root system. Once root rot is prevalent in vegetation it spreads outward and affects even healthy root systems. The wet conditions and stress of the vegetation then can become prime areas for various fungi and insect breeds.

Further author information: (Send correspondence to Margot Accettura)
Margot Accettura: E-mail: msa2123@rit.edu

Autonomous Air and Ground Sensing Systems for Agricultural Optimization and Phenotyping III, edited by J. Alex Thomasson, Mac McKee, Robert J. Moorhead, Proc. of SPIE Vol. 10664, 106640I
 · doi: 10.1117/12.2304045

Although there is still discussion about the reasons why methane causes vegetation stress, it is well-known that the reflectance spectra will be affected. There have been studies showing how the "red-edge" region is highly affected. The "red-edge" is the region between red and near infrared (NIR) reflectance which in healthy vegetation has a sharp slope upward compared to a shallow slope as vegetation senesces. This is because in the red reflectance region chlorophyll in the plant absorbs red light while in the NIR region there is high multiple scattering of radiation because of mesophyll, a leaf cell involved in photosynthesis.[3] An example of healthy and stressed hyperspectral signatures can be seen in Figure 1, where the control vegetation has a steep slope while the two forms of stressed vegetation have shallower slopes. This noticeable stress characteristic has led to previous success in works analyzing the derivative of hyperspectral data to view the peak in the "red-edge" and interpret how methane stress affects the region.[3]

The majority of previous studies into methane stressed vegetation have used large flow rates. These large scale leaks show extreme oxygen deprivation, but in cases of a pipeline leak underground, it is unknown how large a leak is or even that a leak is present until stress is seen on the surface. In order to have an adequate quantity of data to interpret a timeline of leakage, and to determine the reaction vegetation has within that time frame, and account for safety in an indoor location, this experiment utilized a lower flow rate. Instead of an experiment looking at flow rates of approximately 3.5 scfh,[2] this experiment is focusing on flow rates of 1 scfh. This flow rate will provide information on the duration a leak might have been occurring underground before being visible at the surface.

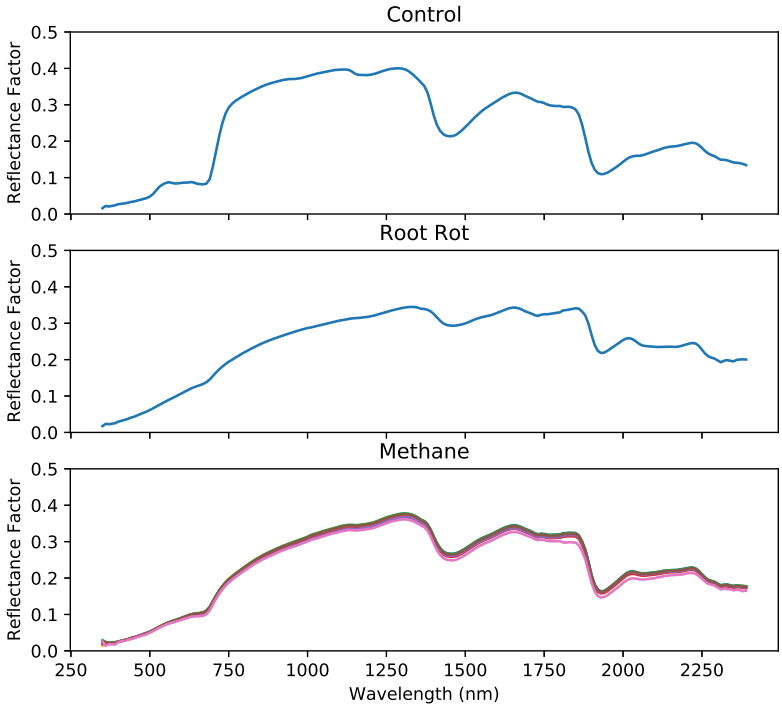

Figure 1: Plot of the mean spectra on the final day of measurements for the three experimental areas. The plot of methane stress shows the mean for each of the six locations taken across the length of the inserted methane pipeline. As can be seen the locations are so similar the location along the pipeline is not taken into account for this study.

2. BACKGROUND

2.1 Hyperspectral Derivative

Hyperspectral analysis in previous work has focused on the derivative of the data.[3] In this experiment the first derivative was implemented by dividing the difference between spectral measurements at each consecutive wavelength by the wavelength sampling interval, in this case the derivative was calculated with a sampling interval of 1 nm. An example of the first derivative of the hyperspectral data for this work is seen in Figure 2. The derivative can be used to more clearly detect spectral signatures than using the hyperspectral radiance or reflectance data. In previous work observing plant stress responses to natural gas, differences between healthy and stressed vegetation have been observed in peaks within the red-edge region along with the derivative ratio between 725 and 702 nm.[3] The wavelengths for the derivative ratio from this previous work was calculated based on a closer look at the red-edge peak where smaller peak regions were noticeable. A closer look at the red-edge peak for this experiment, as shown in Figure 6a, shows a smooth peak so a derivative ratio would not add any information to the analysis of this experiment.

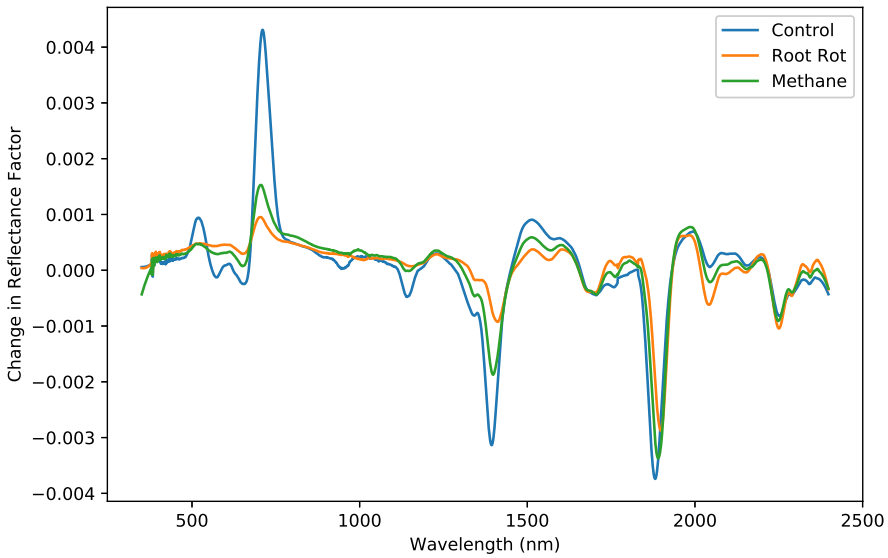

Figure 2: Plot of the first derivative of the mean for the control vegetation, root rot stressed vegetation, and methane stressed vegetation taken on the last day of the collect.

2.2 Physiology Based Indices

2.2.1 Chlorophyll Variation

The chlorophyll content of vegetation is one of the most important parameters for studying vegetation health. In numerous previous studies the normalized difference vegetation index (NDVI) has been used as an analysis of chlorophyll. The NDVI function is stable which allows for comparison over time and, along with the fact that its implementation uses ratios, reduces noise.[4,5] NDVI looks at the difference between visible (VIS) and NIR bands. The chosen bands are flexible so NDVI can be run for a variety of VIS and NIR band combinations.[6] The output of NDVI ranges between -1 and 1, with positive values being healthy vegetation and negative values being stressed vegetation, where ρ is reflectance.

$$NDVI = \frac{\rho_{NIR} - \rho_{VIS}}{\rho_{NIR} + \rho_{VIS}} \tag{1}$$

Other band specific chlorophyll methodologies can be implemented. These other calculations are used to minimize background effects, like the reflectance of the soil. One collection of indices is the Chlorophyll Absorption Ratio Index (CARI). Modified Chlorophyll Absorption Ratio Index, Transformed Chlorophyll Absorption Ratio Index, and Triangular Chlorophyll Index (MCARI, TCARI, and TCI respectively) are all performed as various forms of the CARI calculation. All three of these indices are focused on the visible and red-edge areas of the hyperspectral data. The Soil-Adjusted Vegetation Index (SAVI) was also analyzed along with its variations, the Modified Soil-Adjusted Vegetation Index (MSAVI) and the Optimized Soil-Adjusted Vegetation Index (OSAVI).

Table 1: This table shows the equations for the various chlorophyll physiological indices. ρ is the reflectance at a specific wavelength (nm).

Acronym	Equation
MCARI	$[(\rho_{700} - \rho_{670}) - 0.2(\rho_{700} - \rho_{550})] * (\rho_{700}/\rho_{670})$
TCARI	$3[(\rho_{700} - \rho_{670}) - 0.2(\rho_{700} - \rho_{550})(\rho_{700}/\rho_{670})]$
TCI	$1.2(\rho_{700} - \rho_{550}) - 1.5(\rho_{670} - \rho_{550})\sqrt{\rho_{700} - \rho_{670}}$
SAVI	$\frac{(1+0.5)(\rho_{800} - \rho_{670})}{(\rho_{800} + \rho_{670} + 0.5)}$
MSAVI	$0.5[2 * \rho_{800} + 1 - \sqrt{(2 * \rho_{800} + 1)^2 - 8(\rho_{800} - \rho_{670})}]$
OSAVI	$\frac{(1+0.16)(\rho_{800} - \rho_{670})}{(\rho_{800} + \rho_{670} + 0.16)}$

2.2.2 Water Variation

As oxygen deprivation affects the roots, vegetation is not as effective at retrieving nutrients from water. Previous work has looked at the reflectance of vegetation in terms of water content.[7] In Clevers et al.,[8] they aimed to estimate the canopy water content which is the result of the leaf equivalent water thickness and the leaf area index. There are also physiological indices that can be calculated to look at differences in water content from hyperspectral data. The Normalized Difference Water Index (NDWI) is a ratio similar to NDVI but focused on looking at SWIR bands at 860 and 1240 nm.

$$NDWI = \frac{\rho_{860} - \rho_{1240}}{\rho_{860} + \rho_{1240}} \tag{2}$$

2.2.3 Fluorescence Variation

In previous work,[9,10] the Physiological Reflectance Index (PRI) was used to analyze reflectance of hyperspectral data. The PRI was first presented by Gamon et al.[11] and it is related to the xanthophyll cycle. PRI looks at the reflectance changes near the green part of the spectrum which are related to the xanthophyll cycle, a system connected to the process of photosynthesis. The analysis of the xanthophyll present in the vegetation shows the dynamic changes due to chlorophyll fluorescence. This fluorescence change can lead to early detection of vegetation disturbance.[12] The PRI looks at the relative change betweens bands 531 and 570 nm.

$$PRI = \frac{\rho_{531} - \rho_{570}}{\rho_{531} + \rho_{570}} \tag{3}$$

2.3 Logistic Regression

Logistic regression is a supervised classification technique for analyzing the difference between binary variables. In the analysis of stressed vegetation the binary variables would be unstressed and stressed (0 and 1, respectively). Previous work has used logistic regression to select the optimal bands in the hyperspectral data for locating stressors.[13] In order to determine the optimal bands for differentiation, logistic regression is performed on a per-wavelength basis for all combinations of the hyperspectral wavelengths with a sampling interval of 10 nm. The following equation is used for the logistic regression model, where σ_{ij} is the expected value of the function at wavelengths i and j, β_{0ij} and β_{1ij} are regression coefficients for each combination of wavelengths i and j, X_{ij} are the spectral values at both wavelengths i and j, and ϵ_{ij} is a random error term.

$$\sigma_{ij} = \frac{exp(\beta_{0ij} + \beta_{1ij}X_{ij})}{1 + exp(\beta_{0ij} + \beta_{1ij}X_{ij})} + \epsilon_{ij} \tag{4}$$

In order to determine how well each combination of wavelengths determines stress, an "area under the curve" analysis is implemented. This is the area under the Receiver-Operator Characteristic (ROC) curve. A ROC curve is created by plotting the true-positive fraction (e.g. stressed vegetation identified as stressed) of the logistic regression model by the false-positive fraction of the model (e.g. unstressed vegetation identified as stressed). The area under the ROC curve is a metric that can be used to locate the combination of wavelengths with strong sensitivity for locating vegetation stress. A value of the area under the curve larger than 0.8 shows significant sensitivity.[13]

3. METHODS

This experiment occurred in the winter season so for optimal growth of the turf we implemented the experiment inside the greenhouse at the Rochester Institute of Technology.

3.1 Experimental Set-Up

Three large mixing tubs (24 x 36 x 8 inches) were used as the turf locations for the three experimental variables, methane stress, root rot stress, and control. Four 1/2" holes were placed on the sides of each tub for drainage. A 1/2" diameter copper pipe was placed 4" up the height of the methane tub. Five 1/2" diameter holes were drilled into the copper pipe and were placed facing downwards, aiming towards the bottom of the tub. The copper pipe was surrounded on all sides by pea pebbles. The pebbles were placed around the pipe so the methane would release through the stones and percolate up towards the surface. In order to remain consistent throughout the tubs a layer of pea pebbles was added 4" up the height of the other two tubs. The methane was leaked using a mass flow controller to keep the leak at a consistent speed of 1 scfh. Turfbuilder soil was placed above and below the layer of pea pebbles. The sod, a form of Kentucky Bluegrass, was placed on top of the layer of soil.

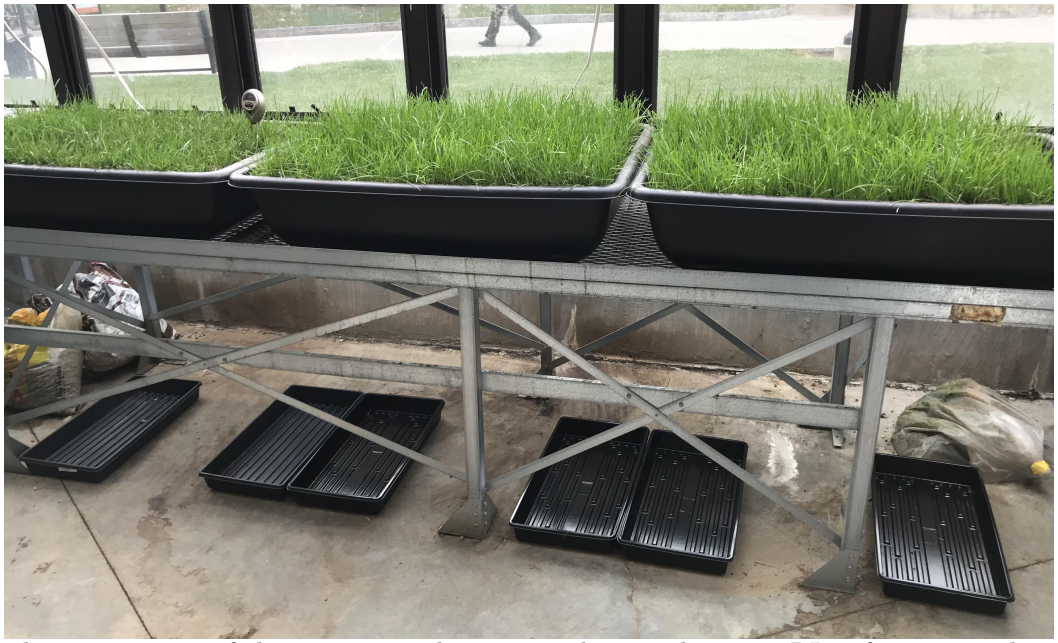

Figure 3: This is an image of the experimental set-up in the greenhouse at RIT after two weeks of growing. From left, the tubs are the methane stressed, root rot stressed, and control. This was prior to the release of the methane when the overlaying turf was rooting.

In order for the sod to root into the soil it had to be kept at optimal conditions for root growth, so the soil temperature, moisture, and pH was monitored daily. The root growth of Kentucky Bluegrass peaks at 60°F. In order to maintain optimal lighting two fluorescent Sylvania T12 grow lamps (Model #046135246715) were placed above the sod. Grow lamps are designed to stimulate plant growth and the ones used in this experiment had a color temperature of 3400 K. To help soil warmth, Vivosun heating mats (Amazon Standard

Identification #B00Y27FJ1C) were placed beneath each tub to provide external heating. They maintained a steady temperature, and heat was distributed evenly across the bottom of the tub. Both the heating mats and glow lamps were placed on a timer to be running from 7 AM to 7 PM local time (Eastern Standard Time). This was to simulate the amount of light present in the summer months. This gave the vegetation enough heat that during daylight hours the soil never fell below 60°F.

3.2 Collection Set-Up

The interior layout of the greenhouse required preparation for data collection, because the greenhouse has multiple walls and a roof constructed of glass. This would lead to sunlight streaming in, which, depending on time of day and weather conditions (e.g. snow accumulation on the roof), would affect the lighting on the scene.

In order to mitigate the issues from stray light, a curtain of black felt was used to isolate the vegetation for image and spectra data collection. At the beginning of daily data collection the black felt curtain was moved on a string above the scene to cover all sides of the tubs. The black felt helped mitigate issues of external lighting, so controlled light sources could be used to create a consistent illumination field on the vegetation. The light sources used were two Sunnex HF Series halogen lamps (Model HF2010). They are movable light sources that could be adjusted to raise the lights and aim them precisely on the scene.

A collection rig was created to keep collection consistent throughout the duration of the experiment. The device was made using various pieces of 80/20, an aluminum building system. It was measured to fit precisely over the tubs with small wheels placed on the bottom so it could be pushed from one tub to another throughout the experiment. The aluminum surface was painted flat black so the interaction of the light shining on the aluminum would not add stray light into the field of view. The Sunnex light sources were attached to the legs so they always moved together from one tub to another. A crossbar spanned the width above the tub and had locations for the two instruments used during this experiment, a point spectrometer and multispectral imager. This allowed the two devices to take measurements at a consistent location for the duration of the experiment.

3.3 Instruments

3.3.1 ASD Spectrometer

The hyperspectral measurements were taken using a FieldSpec Hi-Res Spectroradiometer from ASD, Inc.[14] The spectrometer takes measurements ranging from 350-2500 nm, with a spectral resolution of 3 nm in the visible and NIR and 6 nm in the SWIR, resolution bandwidths which were interpolated to different sampling intervals for analysis. Over the course of the experiment the spectrometer data was collected using a 3°FOV foreoptic. The data was collected at the center line of each tub and was rolled along the length of each tub to collect in six separate positions, each separated by 2 inches.

3.3.2 MicaSense RedEdge

The multispectral measurements were taken using a MicaSense RedEdge camera. The RedEdge camera was placed in the center of the tub for collection. The RedEdge camera has a 47.2°FOV and a resolution of 1280x960. The camera captures images at the five wavelengths shown in Table 2.

Table 2: This table shows the wavelengths captured by the MicaSense RedEdge camera and the bandwidth at the full width half max for each band.

Band	Center Wavelength (nm)	Bandwidth FWHM (nm)
Blue	475	20
Green	560	20
Red	668	10
Red Edge	717	10
Near IR	840	40

4. RESULTS

For the analysis hyperspectral data was smoothed to reduce noise using a Savitzky-Golay filter. This filter involves doing a local polynomial regression to calculate the smoothed value at the center of the filter window[15].

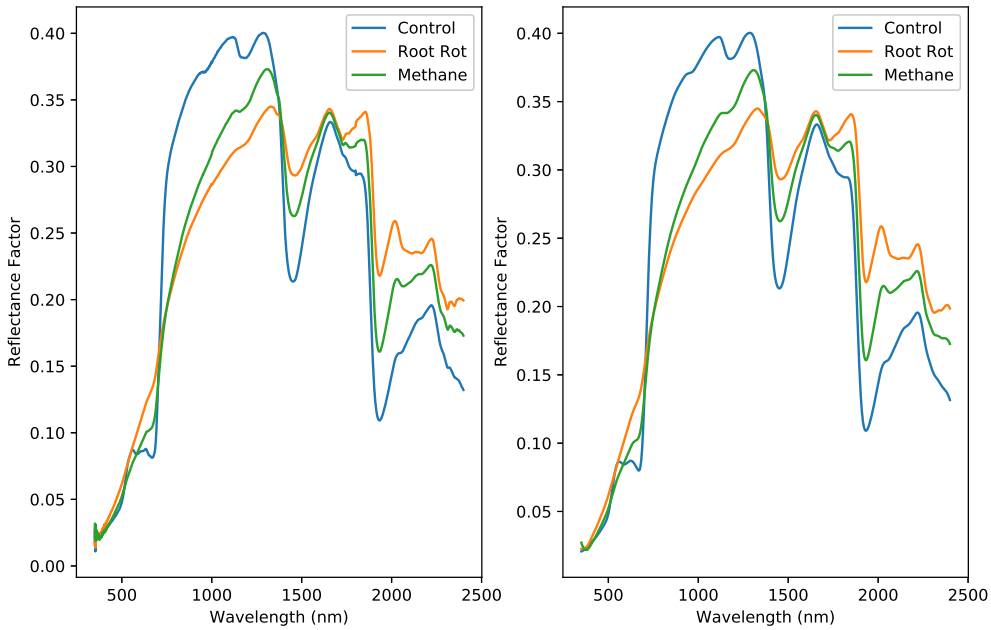

Figure 4: Original plot of the mean spectra (left) next to the smoothed spectra (right). Smoothing is most clearly seen in wavelengths less than 500 nm and greater than 2000 nm.

4.1 Time Series

Over the course of the experiment the spectra of the stressed vegetation changes in a way that shows areas on which to focus when spotting methane stressed vegetation. Initially the vegetation is all similar, with steep red-edge slopes and similar spectral shapes. As the vegetation becomes stressed differences begin to become apparent.

In Figure 5, spectra are shown weekly over the duration of the experiment. The root rot stressed vegetation begins to die before the methane stressed vegetation. The slope in the red-edge region is the first visible change. The slope begins to become shallower as the reflectance values begin to decrease. This occurs in the methane stressed vegetation about two weeks after it is initially seen in the natural stress. After the red-edge slope has begun to decline there is a change in the reflectance values in the SWIR region of the data. By the end of the month long experiment, SWIR reflectance values for both the root rot stressed vegetation and the methane stressed vegetation are higher than the healthy vegetation by the end of the experiment. In healthy vegetation the SWIR range has strong water absorption features, but when vegetation is stressed water absorption no longer conceal absorption features from organic bonds in the vegetation. These absorption features are related to a combination of the protein, lignin, and cellulose of the plant.[16] This is an important take away from the timeline analysis of the experiment. This shows that along with the values of the red-edge decreasing there is also an apparent increase in the values of the SWIR region of the data.

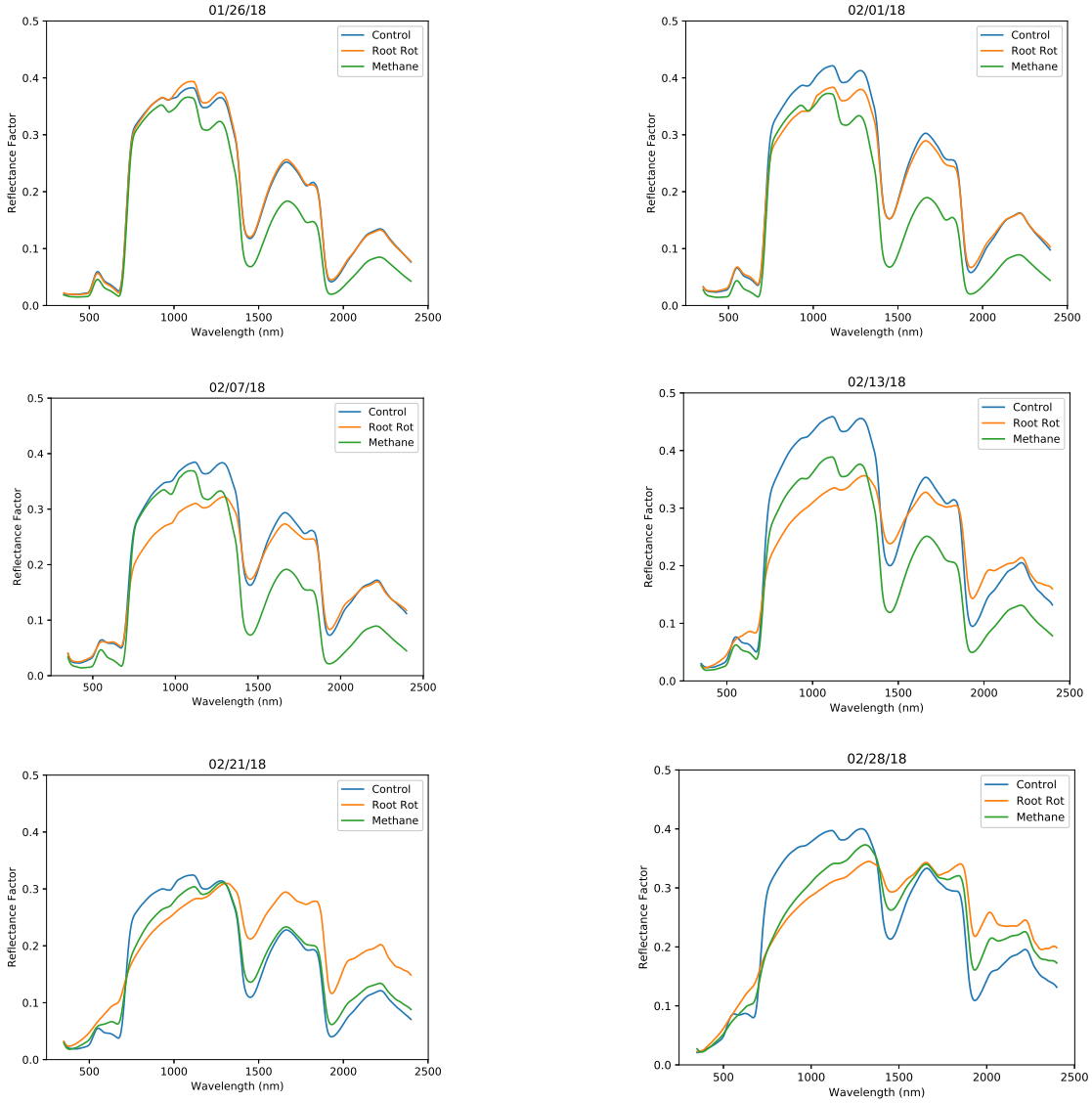

Figure 5: These plots are a time series of the hyperspectral data over the course of the experiment.

4.2 Derivative

The first derivative of the data clearly shows the red edge peak in the data as seen in Figure 2. As this area is a well known indicator of vegetation stress it is focused on in Figure 6a. This plot is of the data from the final day of the experiment. It can be seen that the unstressed vegetation has a much higher peak than the two stressed locations. Between the two forms of stressed vegetation it can be seen that the methane stress still has a higher peak than the root rot stress. This can be explained by the speed with which the natural death occurred compared to the methane death. This timeline difference is shown in Figure 6b. This is a plot of the three peaks for each day of the experiment. The control experiment initially declines then regains health on day 17 of the experiment. This is because the center of the area had begun losing health so the data capture had to react to this event by focusing on a healthy area. It can be seen that while all three tubs begin with similar reflectances the presence of root rot and methane consistently reduce the reflectance. While the root rot begins to show stress within the first week the primary decline in methane stress does not appear until approximately two weeks into the experiment.

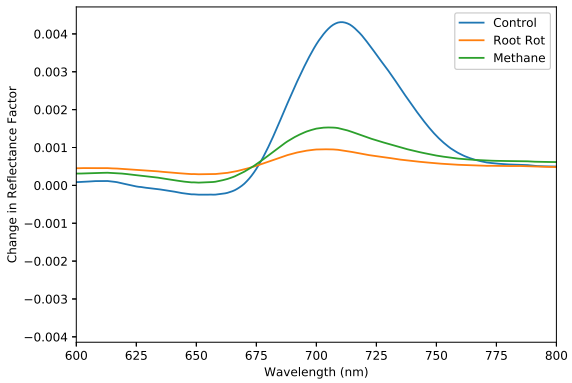

(a) Plot of the first derivative of the mean spectra from 600 to 800 nm. This shows the smoothness of the red-edge peak.

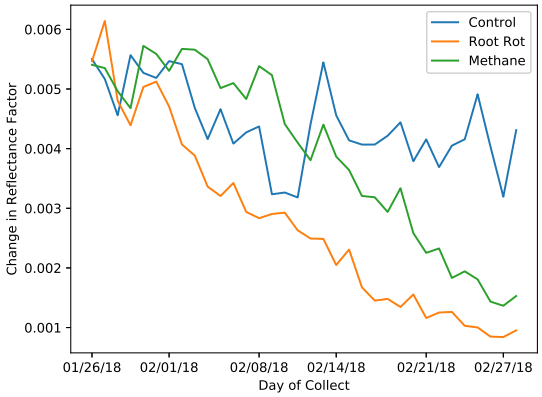

(b) Plot of red-edge peaks over the course of the experiment. Root rot and methane peaks decrease over the course of the experiment, drastically and at a slower pace respectively.

Figure 6: These plots focus on the peak of the red-edge region found in looking at the first derivative of the hyperspectral data.

The full hyperspectral first derivative plot, in Figure 2, also shows a distinct difference in peaks found in the red-edge region and other features in the data. There are two large dips in the SWIR region, with the largest being around 1900 nm. The difference in change in reflectance between the red-edge peak and the SWIR feature is observable. This is an important addition to calculating the first derivative because of its ability to detect wavelengths that might be harder to visualize with the hyperspectral timeline data. The output of this first derivative plot lead to analysis in further sections.

4.3 Physiology Indices

The physiological calculations of the hyperspectral data show a strong difference between stressed and unstressed vegetation along with slighter differences shown between the root rot and methane stressed vegetation. The NDVI function was run looking at the ratio between bands at 680 and 800 nm. In Figure 7a, each area of turf begins with similar NDVI values but the stressed regions begin to deteriorate at different time frames. The root rot NDVI value drops in an almost immediate linear fashion, while the methane stress NDVI value begins a decline after approximately two weeks.

Analysis was also performed to determine the wavelengths for maximum difference in NDI. The NDI ratio was performed for all combinations of wavelengths and the difference between control, root rot, and methane stressed vegetation was analyzed to find the bands which showed the maximum difference. At the end of the experiment when stress was visible from both root rot and methane the two wavelengths with the largest difference in normalized difference values were similar for the two different forms of stress. The calculated wavelengths were 750 and 1910 nm. These wavelengths values correspond to the large peak and large dip in the first derivative plot as seen in Figure 2. The NDI calculation was then performed for those two calculated wavelengths as seen in Figure 7b. These wavelengths lead to a slightly different interpretation than the NDVI function. In the case of NDI, as vegetation becomes more stressed the two wavelengths have a higher ratio. A similar timeline is seen with the methane stressed location increasing in NDI after two weeks and the root rot ratio increasing immediately. The shape of the NDI values over the span of the collect are similar to the shape of NDVI values at 680 and 800 nm but the NDI values are from wavelength values at more pronounced regions of the first derivative plot.

In Table 3 the values of the physiological algorithms are shown for each experimental region on the final day of experimentation. For both NDVI and NDWI the values range from -1 to 1 and the healthy vegetation is the highest value of the three, which is to be expected for non-stressed regions. There is a larger difference between

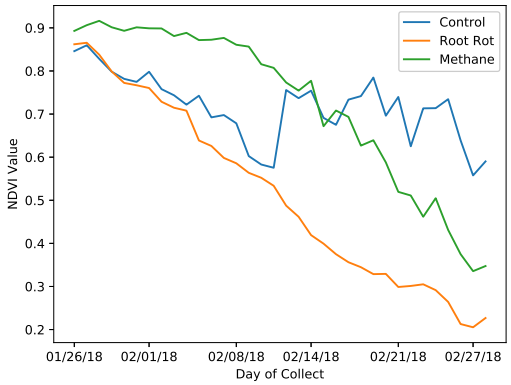

(a) A plot of NDVI values for each day of collect taken at wavelengths of 680 and 800 nm.

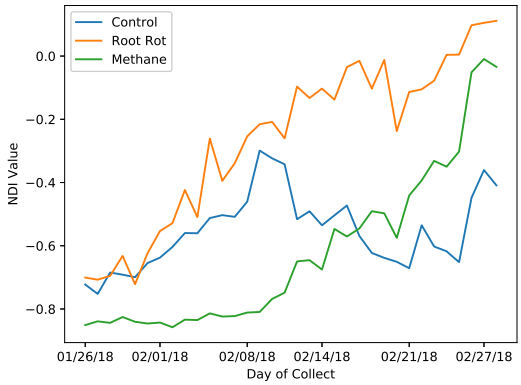

(b) A plot of NDI values for each day of collect taken at wavelengths of 750 and 1910 nm.

Figure 7: The NDVI and NDI plots over the course of the collect

stressed and non-stressed NDVI values than between those variables for NDWI, meaning that the wavelengths for NDVI assessment capture more of a difference than the wavelengths used for NDWI assessment. MCARI, TCARI, SAVI, MSAVI, and OSAVI show the same results as NDVI and NDWI. The control region has the highest result followed by the methane then the natural stress. These results also have a high difference between them as with the NDVI function. This implies that studying chlorophyll is most effective for studying vegetation stress. The only difference is in the TCI function whose value range is opposite with natural stress having the highest value. The PRI equation shows similar results to NDWI where the differences are small between the control, natural, and methane regions. This shows that the xanthyll difference between the three areas is small and that the fluorescence is not greatly affected by methane stress.

Table 3: This table shows the physiological calculations for the final day of data for the three experimental regions of analysis.

Equation	Control	Root Rot	Methane
NDVI	0.590	**0.227**	0.347
MCARI	0.069	**0.008**	0.022
TCARI	0.109	**0.015**	0.042
TCI	0.057	**0.073**	0.064
SAVI	0.408	**0.152**	0.221
MSAVI	0.391	**0.132**	0.195
OSAVI	0.505	**0.195**	0.289
NDWI	-0.055	-0.144	**-0.160**
PRI	-0.071	**-0.104**	-0.097

4.4 Logistic Regression

The logistic regression was calculated for two binary scenarios, control vs root root stress and control vs the methane stress, to find the coefficients of the model. The function was run looking at two band combinations, where the only features used for the model were the two chosen wavelengths. The area under the ROC curve was calculated to determine how sensitive those two bands are because the more sensitive band combinations would be important for use in previous analysis to determine stress in vegetation.

In Figure 8, the combinations of wavelength are plotting against each other, with wavelengths on both axis. This means that the images below are symmetric across the diagonal of the image. The sensitivity of the wavelength combination is shown in the colors on the image. The two band combination that provided the maximum NDI value was plotted as two red circles on the images. As can be seen, the combination of 750 and

1910 nm is in the highest sensitivity ranges on both the root rot and methane comparison images. The control and root rot comparison have various saturated areas of perfect determination. The control and methane stress comparison reach sensitivity close to 0.9 is large areas but has almost no large areas of perfect determination. This can be because of the difference in timing of the root rot and methane stress. In all analysis the root rot caused higher levels of stress to the vegetation compared to the methane stress.

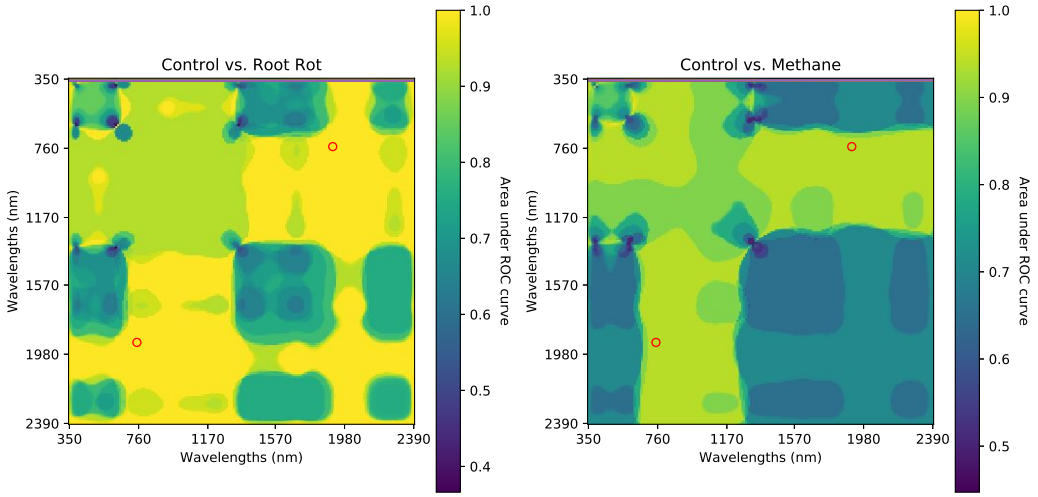

Figure 8: Plots of the area under the curve from a logistic regression of two-band combinations of wavelengths.

5. CONCLUSION

The current analysis has shown the success in using hyperspectral data to determine the presence of stress in vegetation. Methane stress takes longer to be seen compared to natural stress. Natural stress from root rot appears in the hyperspectral data within days while the methane stress appears after approximately two weeks to begins showing stress. This is an important result for understanding the timeline of methane leakage in many utilities. he presence of stress is also most prevalent in the red-edge region of the data because of the decrease of chlorophyll over time. The most important result from this work is the increase in reflectance seen in the SWIR region over time and the location of optimal bands for NDI calculation to be 750 and 1900 nm. The optimal bands were further studied using logistic regression and were found to be highly sensitive. In future analysis of wavelength combination optimization the wavelengths available in MicaSense RedEdge data can be analyzed to determine most affective detection along with the accuracy difference between hyperspectral and multispectral data for vegetation stress determination. This knowledge of optimal band combinations can lead to further exploration of optimal sensors to places onto sUAS systems.

ACKNOWLEDGMENTS

The author would like to acknowledge her fellow authors for their help on this work. The author would also like to thank Nina Raqueño for all of her help. Thanks as well to Jennifer Liedkie of the RIT College of Science and the staff of the RIT greenhouse for giving us space to conduct our experiment.

REFERENCES

[1] Hoeks, J., "Changes in composition of soil air near leaks in natural gas mains.," *Soil Science* **113**(1), 46–54 (1972).

[2] Noomen, M. F., Skidmore, A. K., Van der Meer, F. D., and Prins, H. H., "Continuum removed band depth analysis for detecting the effects of natural gas, methane and ethane on maize reflectance," *Remote Sensing of Environment* **105**(3), 262–270 (2006).

[3] Smith, K., Steven, M., and Colls, J., "Use of hyperspectral derivative ratios in the red-edge region to identify plant stress responses to gas leaks," *Remote sensing of environment* **92**(2), 207–217 (2004).

[4] Huete, A., Didan, K., Miura, T., Rodriguez, E. P., Gao, X., and Ferreira, L. G., "Overview of the radiometric and biophysical performance of the modis vegetation indices," *Remote sensing of environment* **83**(1-2), 195–213 (2002).

[5] Lu, S., Lu, X., Zhao, W., Liu, Y., Wang, Z., and Omasa, K., "Comparing vegetation indices for remote chlorophyll measurement of white poplar and chinese elm leaves with different adaxial and abaxial surfaces," *Journal of experimental botany* **66**(18), 5625–5637 (2015).

[6] Im, J. and Jensen, J. R., "Hyperspectral remote sensing of vegetation," *Geography Compass* **2**(6), 1943–1961 (2008).

[7] Tucker, C. J., "Remote sensing of leaf water content in the near infrared," *Remote sensing of Environment* **10**(1), 23–32 (1980).

[8] Clevers, J. G., Kooistra, L., and Schaepman, M. E., "Estimating canopy water content using hyperspectral remote sensing data," *International Journal of Applied Earth Observation and Geoinformation* **12**(2), 119–125 (2010).

[9] Evain, S., Flexas, J., and Moya, I., "A new instrument for passive remote sensing: 2. measurement of leaf and canopy reflectance changes at 531 nm and their relationship with photosynthesis and chlorophyll fluorescence," *Remote Sensing of Environment* **91**(2), 175–185 (2004).

[10] Wang, H., Chen, J., Lin, H., and Yuan, D., "Research on effectiveness of hyperspectral data on identifying rice of different genotypes," *Remote Sensing Letters* **1**(4), 223–229 (2010).

[11] Gamon, J., Penuelas, J., and Field, C., "A narrow-waveband spectral index that tracks diurnal changes in photosynthetic efficiency," *Remote Sensing of environment* **41**(1), 35–44 (1992).

[12] Krumov, A., Nikolova, A., Vassilev, V., and Vassilev, N., "Assessment of plant vitality detection through fluorescence and reflectance imagery," *Advances in Space Research* **41**(11), 1870–1875 (2008).

[13] Delalieux, S., Van Aardt, J., Keulemans, W., Schrevens, E., and Coppin, P., "Detection of biotic stress (venturia inaequalis) in apple trees using hyperspectral data: Non-parametric statistical approaches and physiological implications," *European Journal of Agronomy* **27**(1), 130–143 (2007).

[14] "ASD FieldSpec Spectroradiometers — ASD Inc.." https://www.asdi.com/products-and-services/fieldspec-spectroradiometers. Accessed: 2018-04-04.

[15] Ruffin, C. and King, R., "The analysis of hyperspectral data using savitzky-golay filtering-theoretical basis. 1," in [*Geoscience and Remote Sensing Symposium, 1999. IGARSS'99 Proceedings. IEEE 1999 International*], **2**, 756–758, IEEE (1999).

[16] Kokaly, R. F., Despain, D. G., Clark, R. N., and Livo, K. E., "Spectral analysis of absorption features for mapping vegetation cover and microbial communities in yellowstone national park using aviris data," (2007).

[17] Yu, D., Lee, S. J., Lee, W. J., Kim, S. C., Lim, J., and Kwon, S. W., "Classification of spectral data using fused lasso logistic regression," *Chemometrics and Intelligent Laboratory Systems* **142**, 70–77 (2015).

[18] Hunt Jr, E. R., Doraiswamy, P. C., McMurtrey, J. E., Daughtry, C. S., Perry, E. M., and Akhmedov, B., "A visible band index for remote sensing leaf chlorophyll content at the canopy scale," *International Journal of Applied Earth Observation and Geoinformation* **21**, 103–112 (2013).